Biophysical Journal

Article

Biophysical Society

Myosin-Induced Gliding Patterns at Varied [MgATP] Unveil a Dynamic Actin Filament

Elina Bengtsson,[1] Malin Persson,[1] Mohammad A. Rahman,[1] Saroj Kumar,[1] Hideyo Takatsuki,[1] and Alf Månsson[1,*]

[1]Department of Chemistry and Biomedical Sciences, Faculty of Health and Life Sciences, Linnaeus University, Kalmar, Sweden

ABSTRACT Actin filaments have key roles in cell motility but are generally claimed to be passive interaction partners in actin-myosin-based motion generation. Here, we present evidence against this static view based on an altered myosin-induced actin filament gliding pattern in an in vitro motility assay at varied [MgATP]. The statistics that characterize the degree of meandering of the actin filament paths suggest that for [MgATP] $\geq$ 0.25 mM, the flexural rigidity of heavy meromyosin (HMM)-propelled actin filaments is similar (without phalloidin) or slightly lower (with phalloidin) than that of HMM-free filaments observed in solution without surface tethering. When [MgATP] was reduced to $\leq$0.1 mM, the actin filament paths in the in vitro motility assay became appreciably more winding in both the presence and absence of phalloidin. This effect of lowered [MgATP] was qualitatively different from that seen when HMM was mixed with ATP-insensitive, N-ethylmaleimide-treated HMM (NEM-HMM; 25–30%). In particular, the addition of NEM-HMM increased a non-Gaussian tail in the path curvature distribution as well as the number of events in which different parts of an actin filament followed different paths. These effects were the opposite of those observed with reduced [MgATP]. Theoretical modeling suggests a 30–40% lowered flexural rigidity of the actin filaments at [MgATP] $\leq$ 0.1 mM and local bending of the filament front upon each myosin head attachment. Overall, the results fit with appreciable structural changes in the actin filament during actomyosin-based motion generation, and modulation of the actin filament mechanical properties by the dominating chemomechanical actomyosin state.

INTRODUCTION

Actin is one of the most abundant eukaryotic proteins (1) and plays key roles in intracellular transport, cell signaling, cellular shape changes, and cell motility (2). These processes involve controlled actin polymerization and depolymerization, as well as actin-myosin interactions (3). Force and motion generation involving different isoforms of myosin II motors and actin filaments (F-actin) is central in all cells and the basis for muscle contraction. In this process, the actin filaments are often viewed as rope-like passive interaction partners (4) despite evidence from spectroscopy, ultrastructural studies, and myosin-binding data indicating that the actin filament structure is dependent on myosin head attachment and the state of the attached myosin motor domains (1,3,5–18).

One way to detect changes in the actin filament state is to monitor the filament flexural rigidity, EI, because E (the Young's modulus) and I (the second moment of inertia of the filament cross section) reflect the intermonomer interaction strength and filament geometry, respectively (18). The flexural rigidity is a measure of the resistance to bending and is often quantified using the persistence length, L_P^f. This is a characteristic correlation length for thermal bending fluctuations along the filament that is related to the flexural rigidity as L_P^f = EI/kT (where k is the Boltzmann constant and T is the absolute temperature). For example, two different flexibility states of actin filaments have been found with different nucleotides bound to the actin subunits in the presence and absence of phalloidin or with and without binding of myosin (5,6,9,10,19–21). Recently, evidence was presented for what seems to be a third flexibility state with even higher flexibility (lower Lp^f), e.g., after cofilin binding (22) or after tethering of the filaments to a surface via proteins that bind along the actin filament side (23). This is consistent with ideas of a strongly dynamic actin filament (1,7,8,24). However, these ideas are not unequivocally supported (25,26) (discussion in (1)), and no marked difference in filament flexibility

Submitted January 11, 2016, and accepted for publication August 22, 2016.

*Correspondence: alf.mansson@lnu.se

Malin Persson's present address is Department of Kinesiology and Physical Education, Karolinska Institutet, Stockholm, Sweden and Department of Kinesiology, McGill University, Montreal, Canada.

Saroj Kumar's present address is Department of Biotechnology, Delhi Technological University, Delhi-42, India.

Editor: Kazuhiro Oiwa.

http://dx.doi.org/10.1016/j.bpj.2016.08.025

between different conditions of myosin-induced actin motility has been observed previously.

In an in vitro motility assay (IVMA), fluorescence-labeled actin filaments are propelled by surface-adsorbed myosin molecules (27,28), or rather, myosin motor fragments such as heavy meromyosin (HMM). A convenient way to describe the statistics of the winding filament paths is to use the path persistence length (Lp^p) (5,29,30), which is the sliding distance after which the memory of the initial tangent angle of the path is effectively lost. Recent results (5,31–33) provide strong evidence that the Lp^p corresponds directly to the Lp^f, i.e., it is determined by the flexural rigidity of the actin filaments. On this basis, we concluded that the flexural rigidity of phalloidin-stabilized actin filaments is reduced to the level of phalloidin-free filaments when the former are propelled by HMM at ionic strengths of $<$100 mM, but not at a higher ionic strength (130 mM) (5). We hypothesized that this discrepancy is due to the failure of myosin-induced structural changes to propagate along the actin filaments at high ionic strength (5). If this is indeed the case, increased density of active myosin heads along the actin filament would be expected to make Lp^p more similar for phalloidin-free and phalloidin-stabilized filaments.

In conflict with the notion that the actin filament paths in an IVMA are fully determined by thermal fluctuations that reflect Lp^f, a recent study (34) suggested that nonthermal fluctuations due to motor-induced forces are important. These forces were largely attributed to motors temporarily acting as cross-linkers between the filament and the surfaces, e.g., as would be expected for cross-bridges in postpowerstroke states. Therefore, a change in the fraction of such motors may be expected to modify the filament paths.

Experiments using lowered MgATP concentrations allowed us to test the above ideas. This intervention reduces the rate of myosin head detachment from actin without changing the attachment rate constant (35), causing an increased density of the attached myosin heads (cf. Fig. 2 in (35)) with the leading head being closer to the filament front. This would facilitate the propagation of myosin-induced structural changes to the free leading end. Furthermore, lowered [MgATP] would increase the fraction of myosin heads in the postpowerstroke state, which is expected to influence nonthermal contributions to the filament trajectories (34). As an alternative approach to increase the fraction of such braking cross-bridges, we mixed functional HMM with HMM that had been made ATP insensitive and noncycling by treatment with N-ethylmaleimide (hereafter termed NEM-HMM).

Unexpectedly, we found a substantial reduction in $L_P{}^p$ by lowering [MgATP] from 1 to 0.05 mM. The observed effect was considerably greater than would be expected according to the hypothesis of improved propagation of structural changes. Together with the effects of HMM and phalloidin on Lp^f, this finding is consistent with three mechanically distinct actin filament states. Among these states, the one with the lowest flexural rigidity (at low [MgATP]) has not, to the best of our knowledge, been observed previously for HMM-propelled filaments. Additionally, our results are consistent with local structural changes occurring in the actin filament upon each myosin head attachment. Finally, we found evidence for a substantially reduced frequency of bursts with an anomalous nonthermal influence (34) on the filament paths at low [MgATP]. This was in contrast to the increase of such an influence after addition of NEM-HMM at 1 mM MgATP. The results are consistent with the idea that reduced Lp^p at lowered [MgATP] to a substantial degree reflects reduced Lp^f, whereas a nonthermal influence relies on the presence of a fraction of noncycling myosin heads. Overall, the results are consistent with a dynamic actin filament whose global and local structure is affected by actin-myosin interaction kinetics. We discuss the mechanisms that promote the formation of a high-flexibility state at low [MgATP] and also consider the properties of this state in relation to key cellular functions and adaptations.

MATERIALS AND METHODS

Ethics statement

All experiments using animal material were approved by the Regional Ethics Committee for Animal Experiments in Linköping, Sweden (reference numbers 58-08, 96-11, and 73-14), and performed in accordance with national and European Union legislations.

Protein preparations and IVMAs

HMM was obtained from fast skeletal muscle myosin, and actin was prepared from acetone powder from skeletal muscle (28,36). Actin filaments were formed by addition of KCl (50 mM) and $MgCl_2$ (2 mM), and in some cases MgATP (3 mM), with no apparent difference in the results. The filaments were treated with tetramethylrhodamine isothiocyanate phalloidin (TRITC-Ph) at molar excess or were fluorescence labeled using N-hydroxysuccinimide rhodamine (NHS-Rh) without phalloidin (5). NEM-HMM was obtained as described previously (37–39). Briefly, HMM (~500 μg/mL) was dialyzed against imidazole-EDTA buffer (10 mM imidazole, 50 mM KCl, 10 mM EDTA, pH 7.0) using a centrifugal concentrator (Vivaspin 2, 28-9322-47; GE Healthcare, Little Chalfont, UK), and treated with NEM (1 mM final concentration; E1271; Sigma-Aldrich, St. Louis, MO) dissolved in ethanol and diluted with the imidazole-EDTA buffer. After incubation for 1 h at 25°C, the NEM-HMM was dialyzed against imidazole-EDTA buffer for removal of excess NEM. The concentration of NEM-HMM was measured using a Bradford assay. The proteins were stored at −80°C until use. The method that we generally use for HMM preparation yields submicromolar concentrations. For some experiments, the HMM concentration was increased to 3–5 μM by a procedure in which HMM (~0.5 μM) was centrifuged at 14,000 × g for 29 min at 4°C using 30 kD cutoff membranes (Nanosep Centrifugal Devices; Pall, Port Washington, NY). The concentrated HMM had similar actin-propelling properties (velocity and fraction of motile filaments) as before the concentration procedure, as tested in separate experiments.

For the IVMAs, glass coverslips functionalized with trimethylchlorosilane (TMCS) (40) were assembled into flow cells that were incubated with HMM (for 2 min), followed by a number of rinsing and blocking steps before addition of 2–10 nM fluorescently labeled actin filaments (30 s). Subsequently, an assay solution containing 0.01–3 mM MgATP, 2.5 mM creatine phosphate, 56 U mL^{-1} creatine kinase, 0.64% methylcellulose, and 115 mM KCl was added. The flow-cell temperature varied between 25.2°C and 29.1°C between different assays. The IVMA conditions were similar to those previously described as important for unbiased studies of path persistence lengths (30). Motility assays with 25% and 30% NEM-HMM out of the total amount of HMM were performed in the presence of 1 mM MgATP, and other experimental conditions were similar to those employed in standard IVMAs.

The image sequences were recorded using an EM-CCD camera (C9100; Hamamatsu Photonics, Hamamatsu, Japan) with a pixel magnification of 0.165 × 0.165 μm^2 per pixel, or a cooled CCD camera (Orca-ER, C4742-95; Hamamatsu Photonics) with a pixel magnification of 0.198 × 0.198 μm^2 per pixel, at frame rates of 5–10 s^{-1} as appropriate. See Supporting Materials and Methods in the Supporting Material for details.

Persistence lengths of actin filament paths and actin filaments in solution

The path persistence length (L_P) of the actin filaments in the IVMA was obtained (5,30) on the basis of the cosine correlation function (CCF), $<\cos(\theta(s) - \theta(0))>$ (where $\theta(s)$ is the instantaneous sliding direction), plotted against the distance (s) along the filament path. An algorithm developed in MATLAB (The MathWorks, Natick, MA) was used to manually track the filaments to obtain $\theta(s)$ and s. Filaments stuck on dead rigor-like HMM heads or filaments undergoing abrupt direction changes (defined by a cutoff value set to 1.5 radians) were excluded before the CCF was fitted (30). The L_P value was obtained from fits of the following equation to the data:

$$\langle \cos(\theta(s)\text{-}\theta(0)) \rangle = \exp(-s/[2 * Lp]). \quad (1)$$

A similar principle was used to obtain the persistence length of actin filaments in solution, aside from using the instantaneous tangent angle at positions s along the filament instead of the tangent angle along the path. For these measurements, actin was diluted to a concentration of 5–40 nM in an assay buffer-based solution but without methylcellulose and MgATP. To create a flow cell of <5 μm thickness, 3–5 μL of the actin sample was sandwiched between a small coverslip (18 × 18 mm^2) and a glass slide. The surfaces were soaked in bovine serum albumin and dried before use. For measurements in the presence of HMM, polyethylene glycol (PEG)-derivatized surfaces (Supporting Materials and Methods) (41) were used to prevent HMM adsorption to the surfaces. In this case, 1–5 μL of the actin+HMM+MgATP sample was sandwiched between the two PEG-coated glass slides (20 × 20 mm^2). In all cases, the flow cells were sealed with nail polish before measurements were obtained at room temperature (20–23°C), and images were recorded with a 0.05 s exposure time.

Statistical analysis, including nonlinear regression

For nonlinear regression and statistical analyses, GraphPad Prism (v. 6.05; GraphPad Software, San Diego, CA) was used. The same program was used to calculate the 95% confidence interval (CI) for a proportion using the modified Wald method. The mean values, without considering the experimental variation at each s-value, were used for nonlinear regression fits to the CCF. This procedure was used due to the decreasing number of data points at increasing values of s and hence an increased uncertainty at higher s-values. If not otherwise stated, the data are given as the mean ± 95% CI.

RESULTS

Evidence suggesting different actin filament flexibility states

Numerical values of Lp^f and Lp^p were obtained at 130 mM ionic strength from exponential fits to the CCF (Eq. 1; Fig. S1). For derivation of Lp^f (Fig. S1 *A*), the CCF was obtained by observing a large number of filaments floating in solution between two closely spaced coverslips. For derivation of Lp^p (Fig. S1 *B*), the CCF was obtained from the paths (Fig. 1) of filaments propelled by HMM in the IVMA (5). In most of the IVMA experiments, the HMM incubation concentration was 120 μg/mL, which is expected to give an isotropic HMM density in the range of 5000–7000 μm^{-2} on TMCS-derivatized surfaces (42–44). Inclusion of methylcellulose in IVMAs has no effect on Lp^p (5). Furthermore, since Lp^f values are similar regardless of whether 1 mM MgATP is present or not (5), MgATP was not included in measurements of Lp^f.

In qualitative agreement with previous results (5), phalloidin-free actin filaments exhibited lower Lp^f and Lp^p values than phalloidin-stabilized filaments (Fig. 2). Furthermore, as was observed previously (5), the Lp^p of phalloidin-labeled filaments at 1 mM MgATP was lower than the Lp^f. For phalloidin-free filaments, on the other hand, the Lp^p and Lp^f were similar (~10 μm). The simplest explanation for these results is that the Lp^p is fully determined by the flexural rigidity of the actin filaments (5,30,33), and that the flexural rigidity of phalloidin-free filaments is unchanged, whereas that of phalloidin-stabilized filaments is reduced upon binding to HMM in an IVMA (5).

When [MgATP] was reduced from 1 mM to 0.05 mM, the velocity decreased 5- to 10-fold (Table S1) but the fraction of motile filaments increased from 60% to 80% (in the absence of blocking actin or other methods for removing dead rigor-like heads) at 1 mM MgATP to almost 100% at 0.05 mM MgATP. Furthermore, the fraction of very short filaments (<<1 μm) increased at low MgATP (Fig. 1 *C*) due to motility-induced fragmentation. It is clear from Fig. 1 that the very short filaments (<<1 μm; *white arrowheads* in Fig. 1) follow distinctly more winding paths than the longer filaments (Movies S1 and S2). We attribute this finding to repeated pivoting of the very short filaments around temporary single surface attachment points via one myosin head (31). Importantly, however, also if filaments shorter than 1 μm were excluded from the analysis, the paths were noticeably more winding on average at low than at high [MgATP] (Fig. 1 *E*; Movies S1 and S2). This is quantitatively reflected in a markedly reduced path persistence length (Figs. 2 and S1 *B*). Thus, Lp^p values at 0.05 mM MgATP, in both the presence and absence of phalloidin,

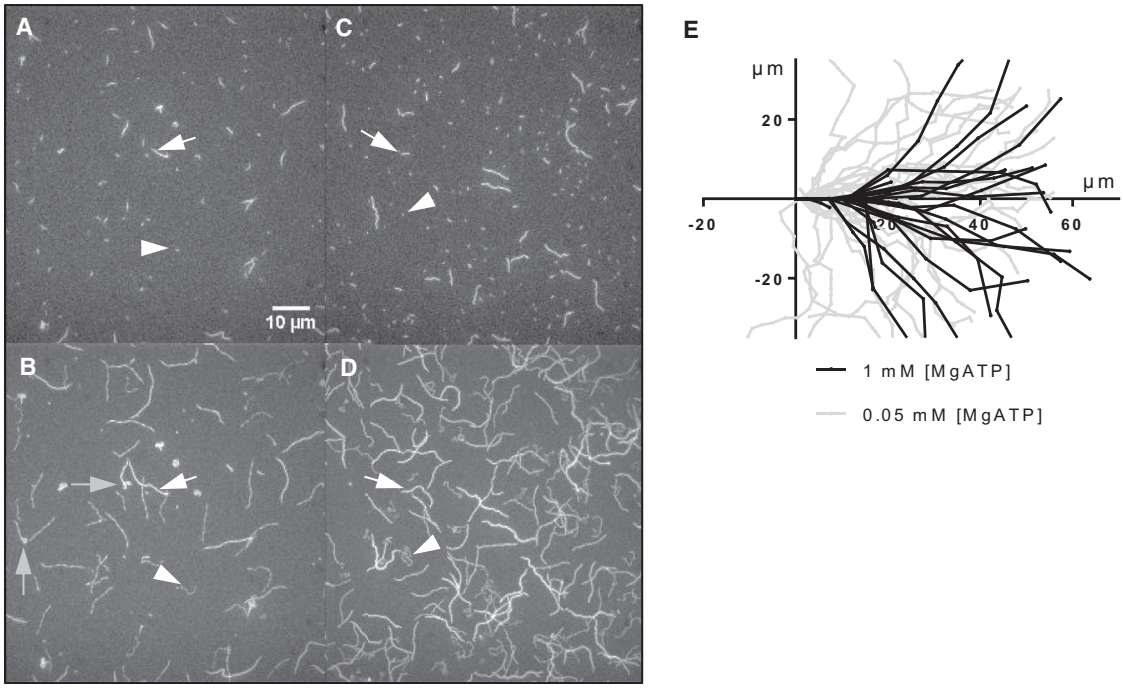

FIGURE 1 Actin filaments propelled by HMM in the IVMA at 1 and 0.05 mM MgATP. (*A*) Fluorescence micrograph (0.2 s) illustrating the starting point of filaments (1 mM MgATP) whose trajectories are illustrated in (*B*). The white arrow and white arrowhead point to typical filaments >1 μm and <1 μm long, respectively. (*B*) Trajectories of filaments at 1 mM MgATP obtained by overlaying five subsequent image frames in a sequence starting with that in (*A*). The white arrow and white arrowhead point to trajectories of corresponding filaments in (*A*). Gray arrows indicate trajectories with abrupt changes in sliding direction toward the end of the observed path due to pinning of filaments on rigor-like dead heads. Such rare trajectories were excluded from the analysis (see text). (*C*) Snapshot as in (*A*) but illustrating the starting point of trajectories in (*D*) (0.05 mM MgATP; arrow and arrowhead as described in *A*). (*D*) Trajectories of filaments at 0.05 mM MgATP obtained by overlaying 20 subsequent image frames in a sequence starting with that in (*C*). A larger number of frames were used to compensate for the lower velocity compared with that obtained at 1 mM MgATP (arrow and arrowhead as described in *B*). (*E*) Trajectories of long (>1 μm) filaments (excluding those with abrupt changes in sliding direction) from (*A*)–(*D*), replotted based on manual tracking in MATLAB. Trajectories at 1 mM MgATP and 0.05 mM MgATP are shown in black and gray, respectively, with the starting point translated to the origin after rotation for the initial sliding direction to be along the horizontal axis. Note that there are more winding paths on average at 0.05 mM MgATP. No methods were used in these experiments to remove or block dead rigor-like heads, e.g., precentrifugation of HMM with ATP and actin or inclusion of blocking actin. All grayscale images were similarly enhanced for contrast and brightness by histogram stretching using ImageJ (71).

were appreciably lower than any value we have previously observed. The filament length distributions were, however, very similar at low and high [MgATP] for filaments included in the quantitative analysis (Fig. S2).

Buckling or related phenomena do not explain low Lp^p at low [MgATP]

The paths of HMM-propelled filaments in the IVMA were governed by the path of the filament front at 0.05 mM MgATP, as was found previously at 1 mM MgATP and also predicted theoretically ((5,31); however, see (34)). This is consistent with the thin appearance of the filament trajectories in Fig. 1 *D*, suggesting that all parts of a filament trace out a similar path. Quantitative evidence is presented in Fig. S3, which shows a <16 nm average lateral deviation from the path of the leading end per micrometer of filament sliding. This magnitude of deviation can be fully explained by thermal fluctuations of the actin filament segments between subsequent myosin-binding sites (cf. equations in (20)) together with uncertainty in the estimates of the filament axis position by Gaussian fits to microscopy images. The results in Fig. S3 were obtained using the long filaments in Fig. 1, *C* and *D*, which were selected for highly curved trajectories to maximize the risk of deviations from a single path. The very small lateral deviations found are in accord with the idea (5,31) that fluctuations of the free leading filament end are the major determinant of the filament paths and therefore of the Lp^p. The findings shown in Figs. 1 *D* and S3 thus argue against appreciable bursts of a nonthermal influence on the filament paths (34). Such bursts would include buckling events, i.e., the emergence of unstable mechanical states of the actin filament with lateral bending into a sinusoidal form of unpredictable amplitude (45) at compressive forces above certain critical values (see below and Supporting Materials and Methods). More generally, the results in Fig. S3 argue against substantial local distortions, independent of origin, that would cause different filament segments to follow different paths (46).

Because myosin heads are in a nucleotide-free, strongly bound, postpowerstroke state for a larger fraction of their actin-attached time when [MgATP] is lowered, we tested

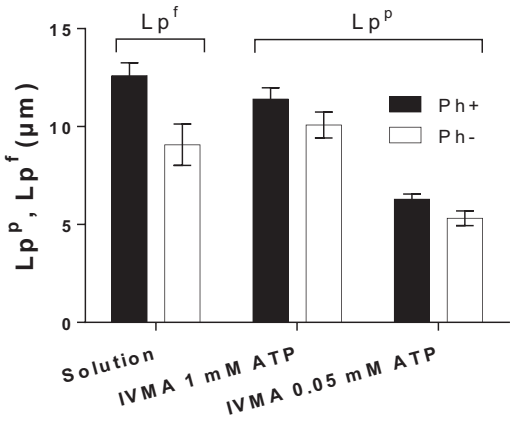

FIGURE 2 Persistence lengths of filaments in solution (Lp^f) and path persistence lengths (Lp^p) with (*black bars*, Ph+) and without (*open bars*, Ph−) phalloidin. Comparison of persistence lengths under different conditions obtained from fits such as those shown in Fig. S1, *A* and *B*. Data (mean ± 95% CI) from at least 200 independent filaments (Lp^f) or filament paths (Lp^p). Only filaments longer than 1 μm were included in the analysis of Lp^p. Other analysis criteria as in (30).

how statically bound heads in a similar state would affect motility and sliding paths. For this purpose, we mixed ordinary HMM with NEM-HMM, which is known (38) to act as a strongly bound, noncycling myosin analog that is not dissociated by MgATP. When motility assays at 1 mM MgATP were performed in the presence of NEM-HMM (added as 30% of total [HMM]), the motility behavior was qualitatively very different from that observed at low [MgATP]. In the latter case, the sliding velocity was substantially reduced compared with that obtained at 1 mM MgATP, but the fraction of motile filaments was increased (see above). In contrast, the inclusion of 30% NEM-HMM caused a smaller reduction in the maximum velocity than in the fraction of motile filaments. Thus, whereas the velocity was reduced by 45% from 7.56 ± 0.30 μm/s to 4.12 ± 0.63 μm/s (n = 30 filaments), the fraction of motile filaments was reduced by 79% from 0.65 ± 0.3 to 0.14 ±0.08 (n = 5 image frames). Very similar results were obtained with 25% NEM-HMM. In further contrast to the effect of lowered [MgATP], different parts of a filament frequently traced out different trajectories in the presence of 25–30% NEM-HMM. These deviations from a single path are readily resolved in standard fluorescence micrographs (Fig. S4) without the need for a detailed analysis as in Fig. S3. Interestingly, similar deviations were present in the supporting movies in a recent study (34), in which the behavior was interpreted as local and random injections of energy by interactions of cycling myosin motors with the actin filament. Here, we attribute the deviations in the presence of noncycling NEM-HMM to buckling events caused by MgATP-insensitive myosin heads that did not detach before exerting large resistive forces. This translates into local compressive forces that are above the critical force of buckling for filaments with a rather large average distance between neighboring actin-attached heads, as expected at high [MgATP]. This explanation is similar to that proposed for nonthermal fluctuations by Weber et al. (34). However, the difference is that we attribute the deviations from one single path (related to a non-Gaussian curvature of the filament) to noncycling cross-bridges, whereas Weber et al. (34) attributed them to cycling cross-bridges that are temporarily cross-linked to the actin filament, e.g., as would be expected for postpowerstroke myosin heads. The latter idea is not immediately consistent with our findings. Whereas we saw a limited number of events with different paths of different filament segments (and non-Gaussian curvature) at 1 mM MgATP, we did not detect such events at 0.05 mM MgATP (Figs. 1 *D* and S3), where the time spent by myosin heads in the postpowerstroke state was appreciably increased.

The above results suggest that the free leading end of the actin filament at low [MgATP] determines the HMM-propelled filament paths. However, for practical reasons, a detailed analysis of filament paths (Fig. S3) could only be applied to a small fraction of all filaments. Therefore, further analysis is required to more definitively rule out the possibility that subtle effects related to buckling or similar events in a large population of filaments contribute to low Lp^p at low [MgATP]. As pointed out above, large angular changes due to buckling are readily identified (e.g., paths with *red arrows* in Figs. 1 *A* and S4) and excluded during either tracking or analysis. In the analysis phase, filaments are excluded if they exhibit angular changes above a certain cutoff value (see Materials and Methods) (30). However, buckling events that cause angular changes below the cutoff are not eliminated. This may distort the distribution of angular updates away from a single Gaussian expected from thermal fluctuations of the leading filament end and increase the width of the distribution (cf. (34)). Therefore, we analyzed several thousands of angular updates (Fig. 3). If occasional buckling events contributed to low Lp^p at 0.05 mM MgATP, there would be an increased number of large and abrupt angular changes between tracking points if no cutoff were used to remove them. Furthermore, one would expect an increased deviation from a single Gaussian of the distribution of angular updates (a non-Gaussian path curvature distribution). In contrast, we found a better single Gaussian fit (Fig. 3, *B* and *C*) at 0.05 mM than at 1 mM MgATP. The lack of systematic deviations from a Gaussian at 0.05 mM MgATP is clear from normally distributed vertical residuals (Fig. 3 *C*) between the fitted curve and experimental data (d'Agostino-Pearson normality test; p = 0.0718) and with the mean value of the residuals indistinguishable from zero (t-test; p = 0.4402). In contrast, at 1 mM MgATP the residuals were nonnormal (p = 0.0033), with an average value different from zero (p = 0.0063), suggesting systematic deviations. Further, the number of large update events in the ranges of [−2.5, −1.5] and [1.5, 2.5] rad in Fig. 3 corresponded to

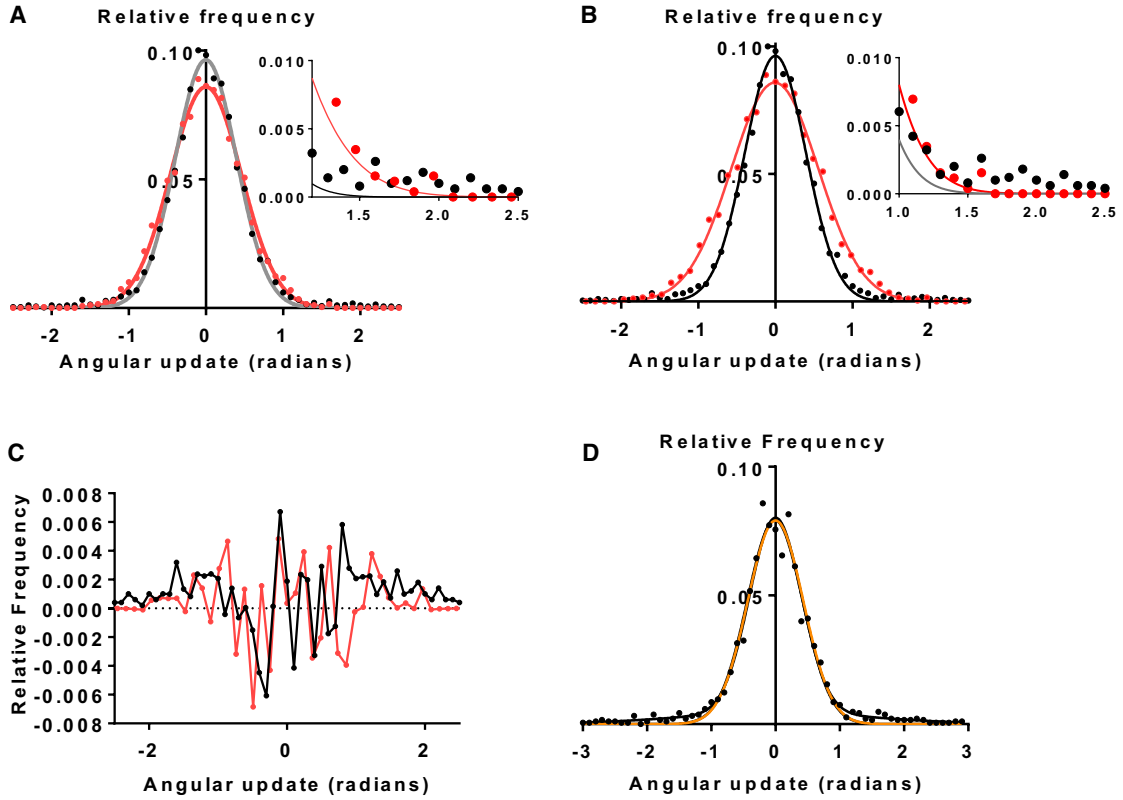

FIGURE 3 Relative frequency distributions for angular updates in the sliding direction between image frames for phalloidin-stabilized actin filaments. (*A*) Data uncorrected for different velocities and interframe times. Black, 1 mM MgATP (time between frames: 0.2 s; sliding velocity 11.73 μm s^{-1}); brighter line and symbols, 0.05 mM MgATP (time between frames: 0.8 s; sliding velocity 1.94 μm s^{-1}). Curves represent Gaussian fits to the data. Total number of events (angular updates): 4970 at [MgATP] = 1 mM and 2588 at [MgATP] = 0.05 mM. Inset: upper tails of distributions shown at higher resolution. (*B*) Data in (*A*) at 0.05 mM [MgATP] were multiplied by $1.2 = \sqrt{11.73x0.2}/_{1.94x0.8}$ to correct for the shorter distance moved between tracking points compared with 1 mM [MgATP] (correction only for the width of the Gaussian, not for the total area under curve). The HMM incubation concentration is 120 μg/mL in (*A*) and (*B*). Note the higher number of large, abrupt changes in the sliding direction (tails of distribution) at high [MgATP] (*black*) compared with low [MgATP] (*brighter line* and *symbols*). (*C*) Vertical residuals (connected by lines for clarity) between data for 1 mM MgATP (*black*) or 0.05 mM MgATP (*bright*) and Gaussian curves in (*B*). Note the larger systematic deviations between the data and Gaussian fit at 1 mM than at 0.05 mM MgATP, particularly for large angular updates (<-1.5 rad and >1.5 rad). For a statistical analysis of residuals, see text. (*D*) Distribution as in (*A*) but for actin filaments propelled by HMM at 1 mM MgATP in the presence of 25–30% NEM-HMM after removal of stationary filaments (Fig. S5, *A* and *B*). Average velocity: 3.87 μm/s. Time between updates: 0.4 s. Bright curve: single Gaussian fit. Black curve: sum of two Gaussians assuming that the mean of each Gaussian component is constant and equal to 0 rad. To see this figure in color, go online.

only 0.35% ± 0.25% (mean ± 95% CI; $n = 2588$) of all events at 0.05 mM MgATP, compared with 2.17% ± 0.41% ($n = 4970$) at 1 mM MgATP. The good fit to a single Gaussian at low [MgATP] is what one would expect for angular updates due to thermal fluctuations of the filament leading end. This is in contrast to what we observed when NEM-HMM (25–30%) was mixed with normal HMM (Fig. 3 *D*). In that case, we found that the sum of two Gaussians gave an appreciably better fit to the data than a single Gaussian. According to the Akaike information criterion (taking into account differences in the sum of squared residuals and applying a penalty for more parameter values in a model), the double Gaussian model was 54 times more likely to fit the data than the single Gaussian. Furthermore, 4.2% ± 0.96% ($n = 1715$) of all update events were in the ranges of [−2.5, 1.5] and [1.5, 2.5] rad, which is significantly higher than in the absence of NEM-HMM (see above). The improved fit with a double compared with a single Gaussian in the presence of NEM-HMM is also evident from the more symmetrical residuals obtained with a double Gaussian (Fig. S5, *C* and *D*). This suggests a non-Gaussian curvature distribution of the actin filament paths as well as a non-Gaussian curvature distribution of the filament itself (34) associated with different paths of different filament segments (Fig. S4).

As a final test to determine whether occasional buckling effects contribute to low Lp^p values at low [MgATP], we performed experiments in which the distance between neighboring myosin heads along the actin filament was varied at 0.05 mM MgATP. This was achieved by lowering the HMM incubation concentration from 120 μg/mL to either 40 μg/mL or 20 μg/mL. These changes reduced the HMM surface density by >35% (40 μg/mL) and >65% (20 μg/mL) (Fig. S6; *dashed lines*), causing an increased

average distance ($<L_f>$; Eq. S4) between attached myosin heads by at least 1.5 and 2.9 times, respectively. The critical buckling force, $F_c \approx \pi^2 Lp^f$ kT/$<L_f>^2$ (Supporting Materials and Methods) is inversely proportional to $<L_f>^2$ ((45,47,48)) and may be estimated to 76 pN and 13 pN at an HMM incubation concentration of 120 and 20 μg/mL, respectively, compared with a maximum force of ~10 pN per myosin head. One would therefore expect an increased risk of buckling and a reduced Lp^p value upon a reduction in the HMM incubation concentration if buckling effects influence Lp^p. In contrast, we found no significant effect (Fig. 4) of the HMM incubation concentration on Lp^p.

We conclude that buckling, as defined above, is extremely rare and has no effect on Lp^p at 0.05 mM MgATP. The buckling frequency is higher at 1 mM MgATP and even higher in the presence of NEM-HMM, but is still uncommon. Below (see Fig. 6), we also consider the possibility that there are random bending effects (other than buckling) close to the leading filament end associated with each myosin head attachment. Such effects may be due to off-axis forces by myosin motors, local conformational changes upon myosin attachment, and bulging of the filament segment between the two leading myosin heads attached to actin. For a detailed account of these possibilities, see Supporting Materials and Methods.

Detailed relationship between Lp^p and [MgATP]

In view of the above results, we felt confident in considering the possibility that actin filament structural states with a lower flexural rigidity dominate during acto-myosin motility at low versus high [MgATP]. If so, one would expect a switch from high to low Lp^p values at critical [MgATP], with fairly constant values above and below this critical concentration. Studies of Lp^p over a range of MgATP concentrations (0.01–3 mM; Fig. 5 *A*), corresponding to a 30-fold variation in sliding velocity (Fig. 5 *B*), were in reasonable agreement with this idea, with an average Lp^p value almost twofold higher at [MgATP] $\geq$ 0.25 mM than at [MgATP] $\leq$ 0.1 mM (*horizontal solid lines* in Fig. 5 *A*). However, the data (Fig. 5 *A*) suggest that the stepwise [MgATP] dependence is superimposed on a graded increase of Lp^p between 0.01 and 1 mM MgATP. Importantly, in a previous study (5), no change in Lp^p was seen when the sliding velocity was reduced from 6 to 3 μm/s by lowering the temperature. This suggests that the effect is specific to reduced [MgATP] and is not a result of reduced velocity per se.

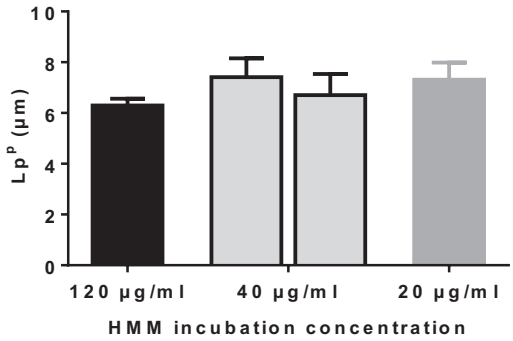

FIGURE 4 Lp^p at 0.05 mM MgATP and different HMM incubation concentrations. One actin preparation was tested at all HMM incubation concentrations and another was tested at 40 μg/mL. Each experimental point (mean $\pm$ 95% CI) was obtained by fitting Eq. 1 to the CCF for >200 independent filament paths. See also Fig. S2.

When [MgATP] approaches zero, the fraction of the actin-attached myosin heads in the nucleotide-free AM state (rigor) approaches one (49), as also captured by modeling (Fig. S7). If the Lp^p value (<5 μm) at the lowest tested [MgATP] is simply due to binding of myosin heads in the absence of nucleotide, one would expect a similar very low persistence length, Lp^f, for actin filaments in solution upon addition of HMM in the absence of MgATP. However, Lp^f was only reduced from 12.67 $\pm$ 0.50 μm in the absence of HMM to 9.21 $\pm$ 1.39 μm (Fig. 5, *A* and *C*) upon equimolar binding of HMM to actin filaments that were floating in solution between closely spaced coverslips. The effect of HMM binding on Lp^f in solution depended on the HMM/actin molar ratio, with the regression coefficient for Lp^f versus HMM concentration (Fig. 5 *C*) being significantly below zero ($p = 0.0078$). We also estimated the Lp^f of actin filaments in solution upon mixing with 0.5 μM HMM and 0.01 mM MgATP, and found that the Lp^f was similar to that obtained for bare actin filaments (Fig. 5 *C*). Increasing the HMM concentration to 4 μM in the presence of MgATP had complex effects (Fig. S8; Movies S4, S5, S6, and S7; see also (6,10))) that precluded reliable estimates of Lp^f. The effects included occasional high-amplitude bending events, presumably due to actin-myosin interactions. These events were associated with filament fragmentation, an effect that was more pronounced at 1 mM than at 0.05 mM MgATP. Additionally, calculations suggested low myosin head labeling of the actin filament (Table S3). Finally, there was evidence for the presence of a fraction of dead (rigor-like) myosin heads (which are likely to always exist in HMM preparations; Fig. S8 *C*; cf. Fig. 1).

Modeling of Lp^p at different [MgATP] and HMM incubation concentrations

As indicated by the data in Fig. 5, the stepwise decrease in Lp^p is superimposed on a continuous decrease with lowered [MgATP]. One possible basis for this continuous effect is local structural changes, e.g., stochastic bending or local conformational changes of the actin filament that occur upon each myosin head attachment (Fig. S9). Such an effect is expected to increase with reduced [MgATP] because the reduced velocity, without a reduction in the myosin head attachment rate, causes more myosin head attachments for a given sliding distance.

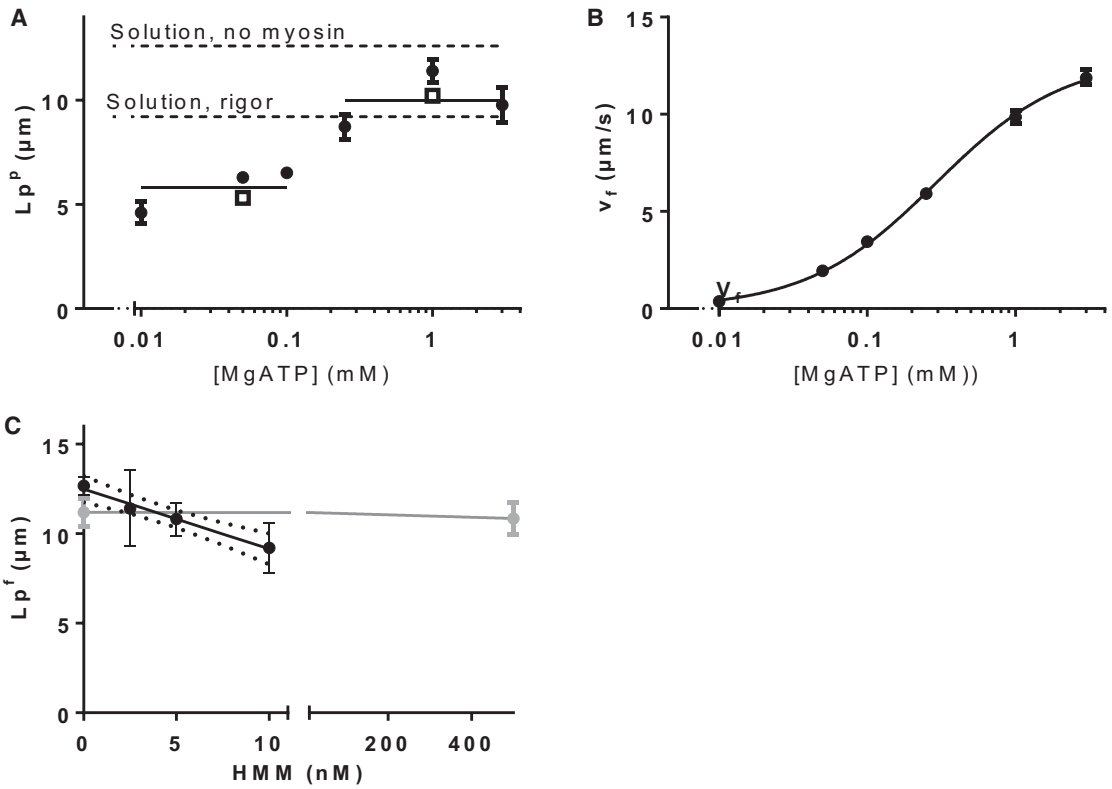

FIGURE 5 Effects of varied [MgATP]. (*A*) Lp^p plotted against [MgATP] on a logarithmic scale obtained after HMM incubation at 120 μg/mL. Each experimental point (mean ± 95% CI) was obtained by fitting Eq. 1 to the CCF for >200 independent filament paths. Solid symbols: phalloidin-stabilized filaments. Open symbols: phalloidin-free filaments. Solid lines: mean Lp^p values for [MgATP] $\leq$ 0.1 mM and [MgATP] $\geq$ 0.25 mM, respectively. Upper and lower dashed lines: Lp^f for phalloidin-stabilized filaments in solution before and after full labeling with HMM in the absence of MgATP. (*B*) Average velocities for phalloidin-stabilized filaments in (*A*) plotted against [MgATP]. (*C*) Effect of HMM binding on Lp^f with actin filaments floating in solution between closely spaced (<5 μm) coverslips (see Materials and Methods). Black symbols and lines: no MgATP. Number of filaments: 0 nM, 809; 2.5 nM, 75; 5 nM, 132; 10 nM, 85. Actin monomer concentration: 10 nM. The regression line (*solid black line*) is shown with the 95% CI (*dotted lines*). Slope: -0.33 ± 0.13 μm nM^{-1}, significantly below zero ($p = 0.0078$). The slope was significantly ($p = 0.0452$) below zero even if the point on the vertical axis was omitted from the linear regression analysis. Gray symbols and line: experiment with ($n = 341$ filaments) and without ($n = 231$ filaments) addition of HMM at 0.5 μM to actin filaments in solution (20 nM) in the presence of 0.01 mM MgATP.

We modeled the mechanism underlying this phenomenon by assuming that each myosin head attachment adds a random angular change, with variance V_{xb}, to that attributed to thermal motion. Under these conditions the apparent persistence length, Lp^{app} (corresponding to Lp^p), would vary with the average distance, $<x>_1$, between subsequent myosin head attachments at the filament front, according to a hyperbolic relationship (Eq. S9):

$$\mathrm{Lp^{app}} = Lp^f \frac{\langle x \rangle_1}{\langle x \rangle_1 + Lp^f V_{xb}}. \quad (2)$$

Here, $<x>_1$ is approximated from experimental data using $<x>_1 = v_f <t>_1$, where v_f is the average sliding velocity and $<t>_1$ is the average time between subsequent myosin head attachments at the filament front (Eq. S2). The quantity $<x>_1$ is correlated with the average steady-state distance, $<L_f>$ (see above) between myosin heads along the actin filament (excluding filament ends; cf. (50)), but the latter value (Eq. S4) is higher. Whereas there are experimental uncertainties in both v_f and $<t>_1$, the changes in $<t>_1$ upon an altered HMM incubation concentration depend primarily on the myosin head density, which is quite reproducible between experiments for TMCS-derivatized surfaces (Fig. S6).

Plots of Lp^p versus $<x>_1$ for all [MgATP] and HMM incubation concentrations are depicted in Fig. 6. The solid horizontal straight lines in Fig. 6 *A* correspond to fits obtained under the assumptions that $V_{xb} = 0$ (i.e., no structural effect of individual head attachments) with one actin filament state at [MgATP] $\leq$ 0.1 mM and another state at [MgATP] $\geq$ 0.25 mM (cf. Fig. 5). Clearly, the fit is poor, with each line being outside the 95% CIs of several individual data points. We also attempted to fit the data assuming the same values of both Lp^f and V_{xb} ($V_{xb} > 0$) at high and low [MgATP] (*gray lines* in Fig. 6 *A*), but the fit was also rather poor in this case (see details below). The results are better reproduced by two mechanisms operating simultaneously: 1) a stepwise decrease in Lp^f when [MgATP] is reduced to <0.25 mM superimposed

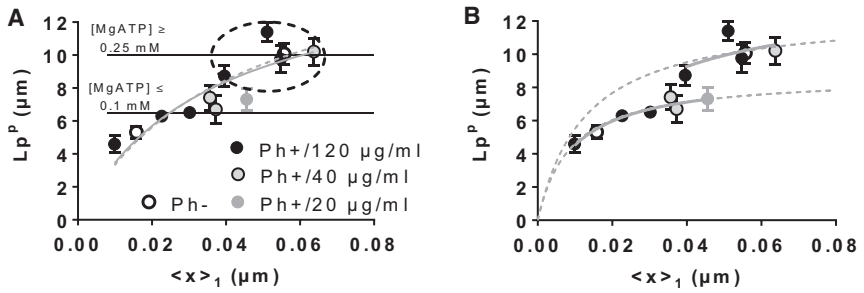

FIGURE 6 Experimental path persistence lengths versus the calculated average sliding distance $<x>_1$ between subsequent myosin head attachments. Solid symbols: with phalloidin (Ph+). Open clear symbols: without phalloidin (Ph−). (*A*) Assumptions that $V_{xb} = 0$ (*black horizontal lines*) or that there is one value of both V_{xb} and Lp^f that is independent of [MgATP] (*gray curved lines*). Black horizontal lines represent the mean value ($Lp^p = Lp^f$ in Eq. 2) of data points at [MgATP] $\geq$ 0.25 mM (data within *dashed ellipse*) and [MgATP] $\leq$ 0.1 mM, respectively. Gray lines represent fits to all data using one value of both V_{xb} and Lp^f, either including the data without phalloidin (*dashed line*) or not (*solid line*). (*B*) Fits of Eq. 2 to the same data as in (*A*) under the assumption that the Lp^f values are different at [MgATP] $\geq$ 0.25 mM and [MgATP] $\leq$ 0.1 mM (*dashed and solid gray lines*). Dashed gray lines represent fits limited to experiments in the presence of phalloidin (Ph+), with the numerical value of V_{xb} obtained from the fit at [MgATP] $\leq$ 0.1 (*lower curve*) and then fixed at this value when fitting Eq. 2 for [MgATP] $\geq$ 0.25 mM (*upper curve*). Solid gray lines represent fits to Ph− and Ph+ data obtained with both Lp^f and V_{xb} varied at [MgATP] $\leq$ 0.1 mM and [MgATP] $\geq$ 0.25. Each experimental point (mean ± 95% CI) was obtained by fitting Eq. 1 to the CCF for >200 independent filament paths. HMM incubation concentration: 120 μg/mL (*black*), 40 μg/mL (*light gray in black circles*), or 20 μg/mL (*dark gray*). For details on the fits, see text and Table S2.

on 2) an additional reduction of Lp^p with reduced [MgATP] due to more myosin head attachments per sliding distance ($V_{xb} > 0$). Based on these assumptions, we first fitted Eq. 2 to all of the data obtained at [MgATP] $\leq$ 0.1 mM, including all HMM incubation concentrations (20–120 μg/mL; cf. Fig. 4). The resulting fit (Fig. 6 *B*) was excellent, giving $Lp^f = 8.69 \pm 1.33$ μm (mean ± 95% CI) and $V_{xb} = 0.0010 \pm 0.0005$. Also, the data point obtained in the absence of phalloidin fell on the line even though it was not included in the fitting procedure. If we then fixed the value of V_{xb} at 0.0010, assuming that this parameter is independent of [MgATP], we obtained a good fit at [MgATP] $\geq$ 0.25 mM with $Lp^f = 12.7 \pm 1.7$ μm. When we instead allowed V_{xb} to vary in the fitting procedure, also at high [MgATP] and including the data point in the absence of phalloidin, we obtained the following parameter values at [MgATP] $\geq$ 0.25 mM (*solid gray lines* in Fig. 6 *B*): $Lp^f = 13.9 \pm 16.4$ μm $V_{xb} = 0.0014 \pm 0.0045$. Whereas these values have appreciable uncertainties, the similarity of the mean V_{xb} value to that obtained at low [MgATP] is consistent with the idea that the numerical value of V_{xb} is independent of $<x>_1$. One may relate the numerical value to real structural changes by realizing that $V_{xb} = 0.001$ corresponds to a standard deviation of 0.03 rad, i.e., a root mean-square change in filament angular direction of 1.8° per myosin head attachment.

Based on the Akaike criterion (see above), two different models at [MgATP] $\geq$ 0.25 mM and [MgATP] $\leq$ 0.1 mM (Fig. 6 *B*) are 13 times more likely to be correct than one given model at different [MgATP] (*gray line* in Fig. 6 *A*). This is in agreement with the overlap of the 95% CIs of 10 out of 12 of the individual data points with the lines representing two models (Fig. 6 *B*), but an overlap with the gray line (one model) in Fig. 6 *A* in only six out of 12 cases. Additionally, the variances of the vertical deviations between the data and the one-model (*gray*, Fig. 6 *A*) and two-model (*blue*, Fig. 6 *B*) fits were 1.15 and 0.753, respectively, i.e., appreciably lower for the two-model case (see Table S2).

As illustrated in Fig. 2 (see also (5,21)), phalloidin increases the flexural rigidity of actin filaments observed floating in solution between two narrowly spaced (<5 μm) coverslips. However, the differences between path persistence lengths in the presence and absence of phalloidin under otherwise similar conditions are considerably smaller (Fig. 1) (5). Therefore, data obtained in the presence and absence of phalloidin fit into the same general picture when a range of conditions are considered as in Fig. 6.

We also attempted to account for the data in Fig. 6 by assuming that the [MgATP] dependence is solely due to the [MgATP] dependence of V_{xb}, i.e. assuming that Lp^f is independent of [MgATP]. However, we obtained poorer fits to the experimental data regardless of whether we assumed a stepwise change of V_{xb} as a function of [MgATP] or a continuous change as a function of $<x>_1$ (Fig. S10).

To summarize, the analyses in Figs. 6 and S10 suggest that 1) different Lp^f values at [MgATP] $\leq$ 0.1 mM (low Lp^f) and [MgATP] $\geq$ 0.25 mM (high Lp^f), and 2) [MgATP]-independent bending of the actin filament upon each myosin head attachment.

DISCUSSION

Key findings in relation to previous work

A central finding of this work was the substantial reduction of Lp^p upon a decrease of [MgATP] to $\leq$0.1 mM. This effect was considerably greater than the decrease in the flexural rigidity (Lp^f) of phalloidin-stabilized actin filaments upon HMM binding in solution. The effect of reduced [MgATP] on Lp^p is not attributed to nonthermal contributions of a type considered recently (34,46). The results we obtained with NEM-HMM instead suggest that such contributions with anomalous filament curvatures (34) are associated with an inhomogeneous HMM population with a high

ratio of statically noncycling to cycling myosin heads. This idea is consistent with the virtual disappearance of anomalous curvatures at low [MgATP]. Under these conditions, the number of cycling myosin heads attached at each given point in time is increased (35) compared with the situation at high [MgATP], whereas the number of dead, rigor-like, nonfunctional heads is not. This increased fraction of cycling heads also explains the larger fraction of motile filaments at low [MgATP].

After considering recently raised issues (34,46) and experimental complications (Figs. 1, 3, 4, and S2–S6), we focused on mechanisms that seem to provide the simplest explanations for the low Lp^p at low [MgATP]. First, the results in Fig. 6 are consistent with two different structural states of the actin filament in the IVMA, with a switch between these states occurring between 0.1 and 0.25 mM MgATP, possibly due to global, cooperative changes in the entire actin filament structure. This is in agreement with previous evidence for different actin filament structural states (7,12,13,24) with cooperative switching between them (1,24,51). Superimposed on the stepwise transition between 0.1 and 0.25 mM MgATP, there was a graded reduction in Lp^p with reduced [MgATP]. The latter effect was correlated with the number of myosin head attachments per sliding distance at the actin filament front (Fig. 6), as well as to the average density of the myosin heads along the filament. One possible basis for this effect is local structural changes (7), e.g., local stochastic bending or local conformational changes in F-actin structure, associated with each myosin head binding independently of the MgATP concentration (Fig. S8). This idea is consistent with the good fits of Eq. 2 to the data obtained by assuming two different Lp^f values but one given value of V_{xb} (Fig. 6 *B*). We also tested alternative models (Fig. 6) that did not involve a change in Lp^f upon reduced [MgATP]. However, none of these models gave as good fit to the data as that obtained with two different Lp^f values at high and low [MgATP].

The results accord with three different structural states of the actin filaments (Fig. S10). These states are characterized by low (8–9 μm), intermediate (~10 μm), or high (>~12 μm) persistence lengths. The state with the highest rigidity exists only in the presence of phalloidin and the absence of myosin binding (Fig. 2; see (5) for details), whereas the state with the lowest flexural rigidity is observed at low [MgATP] in the IVMA and with HMM in solution in the absence of MgATP. The possibility that the state is mechanically similar to that observed upon cofilin binding (22) and strong binding of a number of side-attached actin-binding proteins on a surface (23) needs further consideration.

Possible role of two myosin heads during HMM-induced sliding at low [MgATP]

One may consider the idea that both heads of a given HMM molecule bind sequentially during in vitro sliding at low [MgATP], possibly associated with bending of the filament to accommodate the two heads sterically. Such bending would contribute to the low Lp^p value at low [MgATP]. However, there is previous evidence against two-headed binding under these conditions, based on perfect hyperbolic fits of velocity-[MgATP] data (35). Nor do the data presented here suggest that two-headed binding plays a role. If such binding appreciably contributes to a lowered path persistence length in the motility assay at low [MgATP], one would expect a progressive increase of the effect when [MgATP] is reduced from 0.1 to 0.01 mM. Under these conditions, there would thus be one effect due to the increased number of two-headed attachments and another effect due to the increased number of attachments per sliding distance. We found that the latter effect is sufficient to explain the change in Lp^p in the range of [MgATP] from 0.01 to 0.1 mM (*lower curve* in Fig. 6 *B*). Further, if two-headed binding is important, it would occur only in a fraction of the binding events. As such, it would be expected to cause a double-Gaussian distribution of angular updates in the sliding direction, as observed in the presence of NEM-HMM but not at low [MgATP].

Mechanisms underlying the [MgATP] dependence of Lp^f

Changes in the dominant myosin state (7,12,13) or changes in filament tension alone (52–54) may modify the actin filament structure and affect the flexural rigidity. Therefore, we sought to determine how the predominant chemomechanical actin-myosin states in the IVMA differed at [MgATP] $\leq$ 0.1 mM and [MgATP] $\geq$ 0.25 mM. To that end, we used a recent cross-bridge model (35) that accounts well for a range of experimental findings. Both versions of this model, with linear and nonlinear cross-bridge elasticity, predict that the total fraction of attached myosin heads exhibits an accelerated increase below 0.25 mM MgATP. Furthermore, the fraction of heads in the nucleotide-free state (the AM-state) is predicted to increase above ~50% in the range of 0.1–0.25 mM MgATP. In this context, it is of interest to note that the actin-attacked myosin heads in the model (35) exhibit a wide range of strains, causing local forces on the actin filament (Fig. S9 *C*). This leads us to hypothesize that nucleotide-free AM states exerting a spectrum of forces on the filament, including compressive forces, are mechanistically important for the high-flexibility state at low [MgATP]. However, importantly, as argued above, this effect is not a complication attributed to buckling effects. Instead (see also (5,31,33)), we believe that structural changes at the myosin-binding region of actin allosterically affect nearby filament segments, including the myosin-free and tension-free leading end, reducing the flexural rigidity of this segment.

The idea that compressive forces due to myosin heads in the AM state are important for reducing Lp^f is consistent

with the finding that HMM binding to actin filaments in solution (with some interhead strain) in the absence of MgATP reduces Lp^f, whereas binding of myosin subfragment 1 (one-headed) (10) does not. The idea also fits with the similarity of the Lp^f value at low [MgATP] in the IVMA (from the analysis in Fig. 6) to the Lp^f value of actin filaments floating in solution in the presence of HMM without MgATP (Fig. 5 *C*). In both cases, the AM state dominates and there are compressive forces due either to interhead strain (in solution) or strain due to myosin heads in the postpowerstroke state that counteract propulsive forces by other heads.

Large-amplitude bending events, as observed by us and others (6,10) in the presence of HMM and MgATP in solution, occur with very sparse myosin head binding (cf. Table S3), and various other complexities affect the interpretation (see above and (10)). Nevertheless, one may argue that similar bending events are important in the IVMA. However, given the large amplitude of the bending events in solution and the considerably higher myosin head density in the motility assay, one would then expect the Lp^p to be appreciably lower than the Lp^f. This is in direct conflict with what we observed for phalloidin-free filaments (Fig. 2).

Functional significance and relevance for nanotechnological applications

MgATP concentrations of $\leq$0.1 mM are unlikely to be relevant in cells even under severely fatiguing conditions or hypoxia (55), arguing against adaptive values of the increased flexibility of actin filaments at low [MgATP]. However, one possibility that deserves to be tested in future studies is that this property has been retained during evolution (56) from nonmuscle to muscle actin isoforms. In this context, it is of interest to note that nonmuscle myosin II exhibits low physiological velocities (<1 μm/s) and slow detachment kinetics similar to those of fast skeletal myosin II at low [MgATP] (57). Furthermore, in the same context, it is of interest to note that actin filament disassembly (3) due to interaction with nonmuscle myosin II at the trailing end of nonmuscle cells seems to be important for normal motility of nonmuscle cells. Such disassembly would be facilitated by a reduced filament flexural rigidity, as was recently noted in the presence of cofilin (58). Disassembly is actually also observed (59) in the IVMA when actin filaments are propelled by fast skeletal muscle HMM at [MgATP] $\leq$ 0.1 mM (see also Fig. 1).

The data presented here extend our knowledge (5,60) about how experimental conditions (e.g., filament length, [MgATP], dead myosin heads, and [HMM]; cf. Figs. 1, 2, 3, 4, and 5) affect the path persistence length and path curvature of HMM-propelled filaments. This is important for nanotechnological applications of actin and myosin, such as biosensing (61,62) and parallel computation (63), due to the central role of Lp^p in determining how effectively myosin-propelled actin filaments are guided through nanofabricated networks (32,46,61,64).

CONCLUSIONS

We have further validated a recently developed approach (5,30,31,33) to obtain the actin filament flexural rigidity from the path persistence length, and demonstrated that it provides access to conditions that may not be readily probed otherwise. Using this approach, we have provided evidence for three different actin filament flexibility states, the most flexible of which becomes significantly populated during myosin-induced actin filament sliding at low [MgATP]. The results are in accordance with the idea that actin filaments dynamically switch between a range of structural states depending on, e.g., the imposed tension and binding of myosin heads in the different states. Furthermore, the effect of altered distance between subsequent myosin attachment points suggests that long-range cooperative structural changes are superimposed on short-range changes associated with the attachment of each myosin head. The results also shed light on recently studied phenomena that suggest nonthermal contributions to the filament paths (34). Finally, the data relate to important physiological phenomena and are of value for nanotechnological applications using actin and myosin.

SUPPORTING MATERIAL

Supporting Materials and Methods, ten figures, three tables, and seven movies are available at http://www.biophysj.org/biophysj/supplemental/S0006-3495(16)30747-0.

AUTHOR CONTRIBUTIONS

A.M. designed and conceived the study. E.B., M.P., H.T., M.A.R., and S.K. performed experiments. E.B., M.A.R., and A.M. analyzed data. A.M., E.B., M.P., H.T., M.A.R., and S.K. wrote the manuscript.

ACKNOWLEDGMENTS

We thank Professor S. Tågerud, Dr. M. Bergström, and Dr. S. Karlsson (Linnaeus University) for valuable comments and suggestions, particularly pertaining to methodological issues but also to other aspects of this work. We also thank Dr. T. Korten (Technische Universität Dresden) for advice on surface functionalization.

This work was funded by the Swedish Research Council (projects Nos. 621-2010-5146 and 2015-05290), the Carl Trygger Foundation, the Crafoord Foundation, the faculties of Natural Sciences and Engineering and Health and Life Sciences at Linnaeus University, and the European Union, Future and Emerging Technologies Program within the Seventh Framework Program, grant agreement number 613044 (ABACUS). A.M. is a cofounder, co-owner, and CEO of the startup company ActoSense Biotech AB (Kalmar, Sweden), which aims to develop diagnostic devices based on the aggregation of cytoskeletal elements, particularly actin filaments. A.M. also holds two Swedish patents, one U.S. patent (U.S. 8658 381), and one European Union patent (EP 2 092 343) in this field.

SUPPORTING CITATIONS

References (65–70) appear in the Supporting Material.

REFERENCES

1. Galkin, V. E., A. Orlova, and E. H. Egelman. 2012. Actin filaments as tension sensors. *Curr. Biol.* 22:R96–R101.
2. Pollard, T. D., and J. A. Cooper. 2009. Actin, a central player in cell shape and movement. *Science.* 326:1208–1212.
3. Wilson, C. A., M. A. Tsuchida, …, J. A. Theriot. 2010. Myosin II contributes to cell-scale actin network treadmilling through network disassembly. *Nature.* 465:373–377.
4. Geeves, M. A., and K. C. Holmes. 2005. The molecular mechanism of muscle contraction. *Adv. Protein Chem.* 71:161–193.
5. Vikhorev, P. G., N. N. Vikhoreva, and A. Månsson. 2008. Bending flexibility of actin filaments during motor-induced sliding. *Biophys. J.* 95:5809–5819.
6. Yanagida, T., M. Nakase, …, F. Oosawa. 1984. Direct observation of motion of single F-actin filaments in the presence of myosin. *Nature.* 307:58–60.
7. Prochniewicz, E., T. F. Walseth, and D. D. Thomas. 2004. Structural dynamics of actin during active interaction with myosin: different effects of weakly and strongly bound myosin heads. *Biochemistry.* 43:10642–10652.
8. Kozuka, J., H. Yokota, …, T. Yanagida. 2006. Dynamic polymorphism of single actin molecules in the actin filament. *Nat. Chem. Biol.* 2:83–86.
9. Orlova, A., and E. H. Egelman. 1993. A conformational change in the actin subunit can change the flexibility of the actin filament. *J. Mol. Biol.* 232:334–341.
10. Le Goff, L., F. Amblard, and E. M. Furst. 2002. Motor-driven dynamics in actin-myosin networks. *Phys. Rev. Lett.* 88:018101.
11. Tsaturyan, A. K., N. Koubassova, …, S. Y. Bershitsky. 2005. Strong binding of myosin heads stretches and twists the actin helix. *Biophys. J.* 88:1902–1910.
12. Prochniewicz, E., H. F. Chin, …, E. M. De La Cruz. 2010. Myosin isoform determines the conformational dynamics and cooperativity of actin filaments in the strongly bound actomyosin complex. *J. Mol. Biol.* 396:501–509.
13. Tokuraku, K., R. Kurogi, …, T. Q. Uyeda. 2009. Novel mode of cooperative binding between myosin and Mg2+ -actin filaments in the presence of low concentrations of ATP. *J. Mol. Biol.* 386:149–162.
14. Diensthuber, R. P., M. Müller, …, D. J. Manstein. 2011. Phalloidin perturbs the interaction of human non-muscle myosin isoforms 2A and 2C1 with F-actin. *FEBS Lett.* 585:767–771.
15. Drummond, D. R., M. Peckham, …, D. C. White. 1990. Alteration in crossbridge kinetics caused by mutations in actin. *Nature.* 348:440–442.
16. Yanagida, T., and F. Oosawa. 1975. Effect of myosin on conformational changes of F-actin in thin filament in vivo induced by calcium ions. *Eur. J. Biochem.* 56:547–556.
17. Miki, M., P. Wahl, and J. C. Auchet. 1982. Fluorescence anisotropy of labeled F-actin: influence of divalent cations on the interaction between F-actin and myosin heads. *Biochemistry.* 21:3661–3665.
18. Oosawa, F., and S. Asakura. 1975. Thermodynamics of the Polymerization of Protein. Academic Press, New York.
19. Bugyi, B., G. Papp, …, M. Nyitrai. 2006. Formins regulate actin filament flexibility through long range allosteric interactions. *J. Biol. Chem.* 281:10727–10736.
20. Gittes, F., B. Mickey, …, J. Howard. 1993. Flexural rigidity of microtubules and actin filaments measured from thermal fluctuations in shape. *J. Cell Biol.* 120:923–934.
21. Isambert, H., P. Venier, …, M. F. Carlier. 1995. Flexibility of actin filaments derived from thermal fluctuations. Effect of bound nucleotide, phalloidin, and muscle regulatory proteins. *J. Biol. Chem.* 270:11437–11444.
22. McCullough, B. R., L. Blanchoin, …, E. M. De la Cruz. 2008. Cofilin increases the bending flexibility of actin filaments: implications for severing and cell mechanics. *J. Mol. Biol.* 381:550–558.
23. Crevenna, A. H., M. Arciniega, …, D. C. Lamb. 2015. Side-binding proteins modulate actin filament dynamics. *eLife.* 4:4.
24. Galkin, V. E., A. Orlova, …, E. H. Egelman. 2010. Structural polymorphism in F-actin. *Nat. Struct. Mol. Biol.* 17:1318–1323.
25. Behrmann, E., M. Müller, …, S. Raunser. 2012. Structure of the rigor actin-tropomyosin-myosin complex. *Cell.* 150:327–338.
26. Fujii, T., A. H. Iwane, …, K. Namba. 2010. Direct visualization of secondary structures of F-actin by electron cryomicroscopy. *Nature.* 467:724–728.
27. Kron, S. J., and J. A. Spudich. 1986. Fluorescent actin filaments move on myosin fixed to a glass surface. *Proc. Natl. Acad. Sci. USA.* 83:6272–6276.
28. Kron, S. J., Y. Y. Toyoshima, …, J. A. Spudich. 1991. Assays for actin sliding movement over myosin-coated surfaces. *Methods Enzymol.* 196:399–416.
29. Nitta, T., A. Tanahashi, …, H. Hess. 2006. Simulating molecular shuttle movements: towards computer-aided design of nanoscale transport systems. *Lab Chip.* 6:881–885.
30. Bengtsson, E., M. Persson, and A. Månsson. 2013. Analysis of flexural rigidity of actin filaments propelled by surface adsorbed myosin motors. *Cytoskeleton (Hoboken).* 70:718–728.
31. Duke, T., T. E. Holy, and S. Leibler. 1995. "Gliding assays" for motor proteins: a theoretical analysis. *Phys. Rev. Lett.* 74:330–333.
32. Nitta, T., A. Tanahashi, …, H. Hess. 2008. Comparing guiding track requirements for myosin- and kinesin-powered molecular shuttles. *Nano Lett.* 8:2305–2309.
33. Takatsuki, H., E. Bengtsson, and A. Månsson. 2014. Persistence length of fascin-cross-linked actin filament bundles in solution and the in vitro motility assay. *Biochim. Biophys. Acta.* 1840:1933–1942.
34. Weber, C. A., R. Suzuki, …, E. Frey. 2015. Random bursts determine dynamics of active filaments. *Proc. Natl. Acad. Sci. USA.* 112:10703–10707.
35. Persson, M., E. Bengtsson, …, A. Månsson. 2013. Nonlinear cross-bridge elasticity and post-power-stroke events in fast skeletal muscle actomyosin. *Biophys. J.* 105:1871–1881.
36. Pardee, J. D., and J. A. Spudich. 1982. Purification of muscle actin. *Methods Enzymol.* 85:164–181.
37. Williams, D. L., Jr., L. E. Greene, and E. Eisenberg. 1988. Cooperative turning on of myosin subfragment 1 adenosinetriphosphatase activity by the troponin-tropomyosin-actin complex. *Biochemistry.* 27:6987–6993.
38. Swartz, D. R., and R. L. Moss. 1992. Influence of a strong-binding myosin analogue on calcium-sensitive mechanical properties of skinned skeletal muscle fibers. *J. Biol. Chem.* 267:20497–20506.
39. Kuhn, J. R., and T. D. Pollard. 2005. Real-time measurements of actin filament polymerization by total internal reflection fluorescence microscopy. *Biophys. J.* 88:1387–1402.
40. Sundberg, M., J. P. Rosengren, …, A. Månsson. 2003. Silanized surfaces for in vitro studies of actomyosin function and nanotechnology applications. *Anal. Biochem.* 323:127–138.
41. Papra, A., N. Gadegaard, and N. B. Larsen. 2001. Characterization of ultrathin poly(ethylene glycol) monolayers on silicon substrates. *Langmuir.* 17:1457–1460.
42. Persson, M., N. Albet-Torres, …, M. Balaz. 2010. Heavy meromyosin molecules extending more than 50 nm above adsorbing electronegative surfaces. *Langmuir.* 26:9927–9936.

43. Balaz, M., M. Sundberg, …, A. Månsson. 2007. Effects of surface adsorption on catalytic activity of heavy meromyosin studied using a fluorescent ATP analogue. *Biochemistry.* 46:7233–7251.

44. Sundberg, M., M. Balaz, …, A. Månsson. 2006. Selective spatial localization of actomyosin motor function by chemical surface patterning. *Langmuir.* 22:7302–7312.

45. Howard, J. 2001. Mechanics of Motor Proteins and the Cytoskeleton. Sinauer Associates, Sunderland, MA.

46. Ishigure, Y., and T. Nitta. 2015. Simulating an actomyosin in vitro motility assay: toward the rational design of actomyosin-based microtransporters. *IEEE Trans. Nanobioscience.* 14:641–648.

47. Timoshenko, S. P., and J. M. Gere. 1961. Theory of Elastic Stability, 2nd ed. McGraw-Hill, New York.

48. Brangwynne, C. P., F. C. MacKintosh, …, D. A. Weitz. 2006. Microtubules can bear enhanced compressive loads in living cells because of lateral reinforcement. *J. Cell Biol.* 173:733–741.

49. Cooke, R., and K. Franks. 1980. All myosin heads form bonds with actin in rigor rabbit skeletal muscle. *Biochemistry.* 19:2265–2269.

50. Uyeda, T. Q., S. J. Kron, and J. A. Spudich. 1990. Myosin step size. Estimation from slow sliding movement of actin over low densities of heavy meromyosin. *J. Mol. Biol.* 214:699–710.

51. Prochniewicz, E., Q. Zhang, …, D. D. Thomas. 1996. Cooperativity in F-actin: binding of gelsolin at the barbed end affects structure and dynamics of the whole filament. *J. Mol. Biol.* 260:756–766.

52. Uyeda, T. Q., Y. Iwadate, …, S. Yumura. 2011. Stretching actin filaments within cells enhances their affinity for the myosin II motor domain. *PLoS One.* 6:e26200.

53. Hayakawa, K., H. Tatsumi, and M. Sokabe. 2011. Actin filaments function as a tension sensor by tension-dependent binding of cofilin to the filament. *J. Cell Biol.* 195:721–727.

54. Greene, G. W., T. H. Anderson, …, J. N. Israelachvili. 2009. Force amplification response of actin filaments under confined compression. *Proc. Natl. Acad. Sci. USA.* 106:445–449.

55. Allen, D. G., and C. H. Orchard. 1987. Myocardial contractile function during ischemia and hypoxia. *Circ. Res.* 60:153–168.

56. Mounier, N., and J. C. Sparrow. 1997. Structural comparisons of muscle and nonmuscle actins give insights into the evolution of their functional differences. *J. Mol. Evol.* 44:89–97.

57. Yengo, C. M., Y. Takagi, and J. R. Sellers. 2012. Temperature dependent measurements reveal similarities between muscle and non-muscle myosin motility. *J. Muscle Res. Cell Motil.* 33:385–394.

58. McCullough, B. R., E. E. Grintsevich, …, E. M. De La Cruz. 2011. Cofilin-linked changes in actin filament flexibility promote severing. *Biophys. J.* 101:151–159.

59. Hooft, A. M., E. J. Maki, …, J. E. Baker. 2007. An accelerated state of myosin-based actin motility. *Biochemistry.* 46:3513–3520.

60. Takatsuki, H., E. Bengtsson, and A. Månsson. 2013. Flexural rigidity of actin bundles propelled by heavy meromyosin. *Biophys. J.* 104:649a.

61. Lard, M., L. Ten Siethoff, …, A. Månsson. 2013. Ultrafast molecular motor driven nanoseparation and biosensing. *Biosens. Bioelectron.* 48:145–152.

62. Korten, T., A. Månsson, and S. Diez. 2010. Towards the application of cytoskeletal motor proteins in molecular detection and diagnostic devices. *Curr. Opin. Biotechnol.* 21:477–488.

63. Nicolau, D. V., Jr., M. Lard, …, D. V. Nicolau. 2016. Parallel computation with molecular-motor-propelled agents in nanofabricated networks. *Proc. Natl. Acad. Sci. USA.* 113:2591–2596.

64. Nitta, T., and H. Hess. 2012. Effect of path persistence length of molecular shuttles on two-stage analyte capture in biosensors. *Cell. Mol. Bioeng.* 6:109–115.

65. Klinth, J., A. Arner, and A. Månsson. 2003. Cardiotonic bipyridine amrinone slows myosin-induced actin filament sliding at saturating [MgATP]. *J. Muscle Res. Cell Motil.* 24:15–32.

66. Gillespie, D. 1976. A general method for numerically simulating the stochastic time evolution of coupled chemical reactions. *J. Comput. Phys.* 22:403–434.

67. Woledge, R. C., N. A. Curtin, and E. Homsher. 1985. Energetic Aspects of Muscle Contraction. Academic Press, London.

68. Välimaa, L., K. Pettersson, …, T. Lövgren. 2004. Quantification of streptavidin adsorption in microtitration wells. *Anal. Biochem.* 331:376–384.

69. Nyitrai, M., R. Rossi, …, M. A. Geeves. 2006. What limits the velocity of fast-skeletal muscle contraction in mammals? *J. Mol. Biol.* 355:432–442.

70. Kojima, H., A. Ishijima, and T. Yanagida. 1994. Direct measurement of stiffness of single actin filaments with and without tropomyosin by in vitro nanomanipulation. *Proc. Natl. Acad. Sci. USA.* 91:12962–12966.

71. Schneider, C. A., W. S. Rasband, and K. W. Eliceiri. 2012. NIH Image to ImageJ: 25 years of image analysis. *Nat. Methods.* 9:671–675.